Received: 21 May 2022 | Accepted: 12 October 2022

DOI: 10.1111/2041-210X.14016

Methods in Ecology and Evolution

RESEARCH ARTICLE

Intelligent sampling of high-dimensional joint mobility space for analysis of articular function

Peter J. Bishop[1,2] | Robert J. Brocklehurst[1] | Stephanie E. Pierce[1]

[1]Museum of Comparative Zoology and Department of Organismic and Evolutionary Biology, Harvard University, Cambridge, Massachusetts, USA

[2]Geosciences Program, Queensland Museum, Brisbane, Queensland, Australia

Correspondence
Peter J. Bishop
Email: pbishop@fas.harvard.edu

Funding information
United States National Science Foundation, Grant/Award Number: DEB-1754459 and EAR-2122115; William F. Milton Fund (Harvard University)

Handling Editor: Pablo Duchen

Abstract

1. Studies of joint structure and function have played a central role in understanding palaeobiology and major functional transitions in evolutionary history, where fossilized hard parts (e.g. bones) are often all that remain. Current digital methods for quantifying articular function depend on exhaustively sampling all possible joint poses, but this is computationally intensive, becoming prohibitively so with more degrees of freedom. This has impeded more sophisticated analyses or broader application of these methods to more diverse questions and species.
2. The present study introduces 'APSE' (*A*ccelerated *P*ose *S*earching with *E*lectrostatics), an iterative algorithm for rapidly and intelligently sampling high-dimensional joint pose space to quantify articular function and mobility. Key features of the algorithm are: known viable joint poses inform the search for new poses in successive generations; the search preferentially targets under-explored regions of pose space, while avoiding over-explored regions; large swaths of inviable pose space are never evaluated, thus minimizing wasted time; and parallelizability. The efficacy of the algorithm was benchmarked with diverse theoretical and biological joints. As a case study to demonstrate its utility, APSE was used to investigate mobility in the enigmatic shoulder joint of the extinct 'pelycosaur'-grade synapsid *Dimetrodon*, the function of which has been widely debated.
3. APSE produces high-dimensional joint mobility assessments with greater precision than state-of-the-art exhaustive sampling methods. More viable poses are identified at a greater sampling density, but in a fraction of the time taken by current methods (hours, not days or weeks). Results for *Dimetrodon* shoulder mobility indicate strong coupling between most degrees of freedom across the joint's full range of motion, a stark contrast to the flexible shoulder of most extant tetrapods.
4. APSE provides a time-efficient means to quantitatively measure articular function and mobility, especially when more degrees of freedom are considered. By greatly reducing computational requirements, APSE lowers the barrier to researchers seeking to undertake more complex or more numerous analyses of articular function in modern and extinct animals. This will accelerate the pace of research in comparative or evolutionary analyses of joint and animal function.

KEYWORDS
articular function, *Dimetrodon*, evolutionary biomechanics, joint mobility, range of motion, sampling algorithm

1 | INTRODUCTION

Deciphering skeletal articulation and movement at joints is central to understanding anatomy and functional morphology, and to that end investigation of joint function has played a key role in studies of animal biology and evolution. This is particularly true for extinct species, where fossil bones, other mineralized tissues and their articular surfaces are frequently all that remains. Analysis of joint structure and function has long played a prominent role in interpreting the palaeobiology of species, including limb and neck posture (Paul, 1998; Richards et al., 2021; Stevens & Parrish, 1999), appendage, tail and foot function (Béchard et al., 2014; Bicknell et al., 2022; Clark et al., 2020; Mallison, 2010; Ostrom, 1969; Senter & Robins, 2005), and maximum running speed (Gatesy et al., 2009). Moreover, joint function has been critical for framing and testing hypotheses of major evolutionary transitions. These include shifts in locomotor posture in synapsids (Jenkins Jr., 1971; Kemp, 1978; Lai et al., 2018) and archosaurs (Bonaparte, 1984; Demuth et al., 2020; Parrish, 1986), the origin of terrestriality in tetrapods (Molnar et al., 2021; Pierce et al., 2012), and the advent of forelimb-powered flight in birds (Gatesy & Baier, 2005; Heers & Dial, 2012).

A key element to understanding joint function in extant and extinct vertebrates is joint kinematics and mobility, and methods for quantitatively investigating these aspects have advanced considerably in recent years (Manafzadeh & Gatesy, 2022). Presently, the range of motion in each degree of freedom (DOF), and potential interactions between DOFs, is explored via virtual methods that involve manipulation of digital facsimiles of joint structures (e.g. triangulated mesh models). This process ultimately produces a multi-dimensional 'mobility map' of joint pose space, delimiting sets of poses that are viable (achievable) and inviable. In these maps, each coordinate corresponds to a combination of joint rotations (and/or translations) that satisfies one or more viability criteria—that is, conditions believed to reflect biological constraints on movement (e.g. avoiding bone collision). The current state-of-the-art in digital mobility assessment (Brocklehurst et al., 2022; Manafzadeh & Gatesy, 2021; Manafzadeh & Gatesy, 2022; Manafzadeh & Padian, 2018) involves an exhaustive search of pose space, traversing each DOF in fixed increments and querying pose viability at every possible combination of rotations (and sometimes translations) within pre-defined limits on DOF excursion.

Exhaustive sampling approaches offer a rigorous, reproducible and quantitative assessment of joint mobility and its complexity in multiple dimensions. However, a key drawback is the large processing time involved in systematically evaluating all pose combinations; using typically employed sampling and mesh resolutions, this frequently amounts to tens of hours to multiple days. Additionally, much of the processing time ends up being wasted if large parts of pose space are inviable. These problems are exacerbated as more DOFs are involved, where the number of poses to evaluate grows exponentially (Manafzadeh & Gatesy, 2022), quickly resulting in intractable computational requirements (several days to several weeks, or more). Avoiding this obstacle currently necessitates sacrificing one or more aspects of analysis accuracy or precision. This includes reduction of sampling increment resolution (e.g. sampling every 10° instead of every 5°; Brocklehurst et al., 2022), restricting the number of DOFs considered (e.g. rotations only), using lower resolution digital models, or restricting the number of viability criteria to evaluate (lowering computational load per pose evaluation). Depending on the research question, these may impact how informative the results obtained are for biological interpretations. For example, currently practical sampling resolutions enable only the coarsest assessment of how translations and rotations may interact throughout movement, despite the importance of translations becoming increasingly apparent (Manafzadeh & Gatesy, 2021; Richards et al., 2021). Collectively, these computational limitations act as substantial barriers to investigators seeking to understand complex joint morphologies, particularly within the scope of comparative or evolutionary analyses that involve numerous joints or species.

This paper introduces 'APSE' (*A*ccelerated *P*ose *S*earching with *E*lectrostatics), an algorithm that addresses the aforementioned problems. APSE intelligently samples high-dimensional joint pose space to generate an envelope of viable joint configurations in substantially less time than it would take using exhaustive sampling. The proportion of that time spent evaluating inviable poses is diminished, allowing greater dedication of effort towards producing a higher-resolution quantification of rotational and translational mobility. After outlining the algorithm's implementation and demonstrating its effectiveness in diverse situations, as a case study it is applied to the shoulder (glenohumeral) joint of 'pelycosaur'-grade synapsids. These early forerunners of mammals are a key part of the evolutionary transition from sprawling to erect postures, but their bizarre 'screw shaped' glenohumeral morphology lacks any analogue among extant species, inspiring debate for over a century (Haines, 1952; Jenkins Jr., 1971; Romer, 1922; Watson, 1917). Hypotheses of coupled rotation and translation at this joint remain to be rigorously tested in 6 DOFs; APSE provides a solution to this problem. More broadly, the huge increase in sampling speed offered by APSE can greatly quicken the pace of investigation of joint function across the evolutionary history of animals.

2 | MATERIALS AND METHODS

2.1 | Algorithm description and implementation

A schematic overview of the user workflow implementing APSE is given in Figure 1. A brief outline of the logic underlying APSE is provided here, with a detailed description provided in the Supporting Information. The algorithm emulates how an investigator would manually explore joint mobility with physical specimens, by starting with a known viable pose and iteratively working towards new, adjacent regions of pose space to assess viability over successive generations. Currently known viable poses inform where the algorithm searches in the future. Enhancing this basic process is a mechanism designed to preferentially target under-explored regions of pose space and avoid over-explored regions, based on electrostatic repulsion. As described by Coulomb's Law; 'particles' (ordered *N*-tuples in pose space, corresponding to the *N* DOFs under consideration) tend to be repelled away from currently known viable locations in pose space, increasing the likelihood of reaching under- or unexplored regions of pose space. The user supplies the bounds on each DOF over which to search, one or more criteria for evaluating pose viability, and an initial seed point from which to commence the search, which is a priori known to be viable. Several parameters govern algorithm behaviour, the most important being *k*, which dictates the maximum amount of particle movement along any one dimension of pose space in a

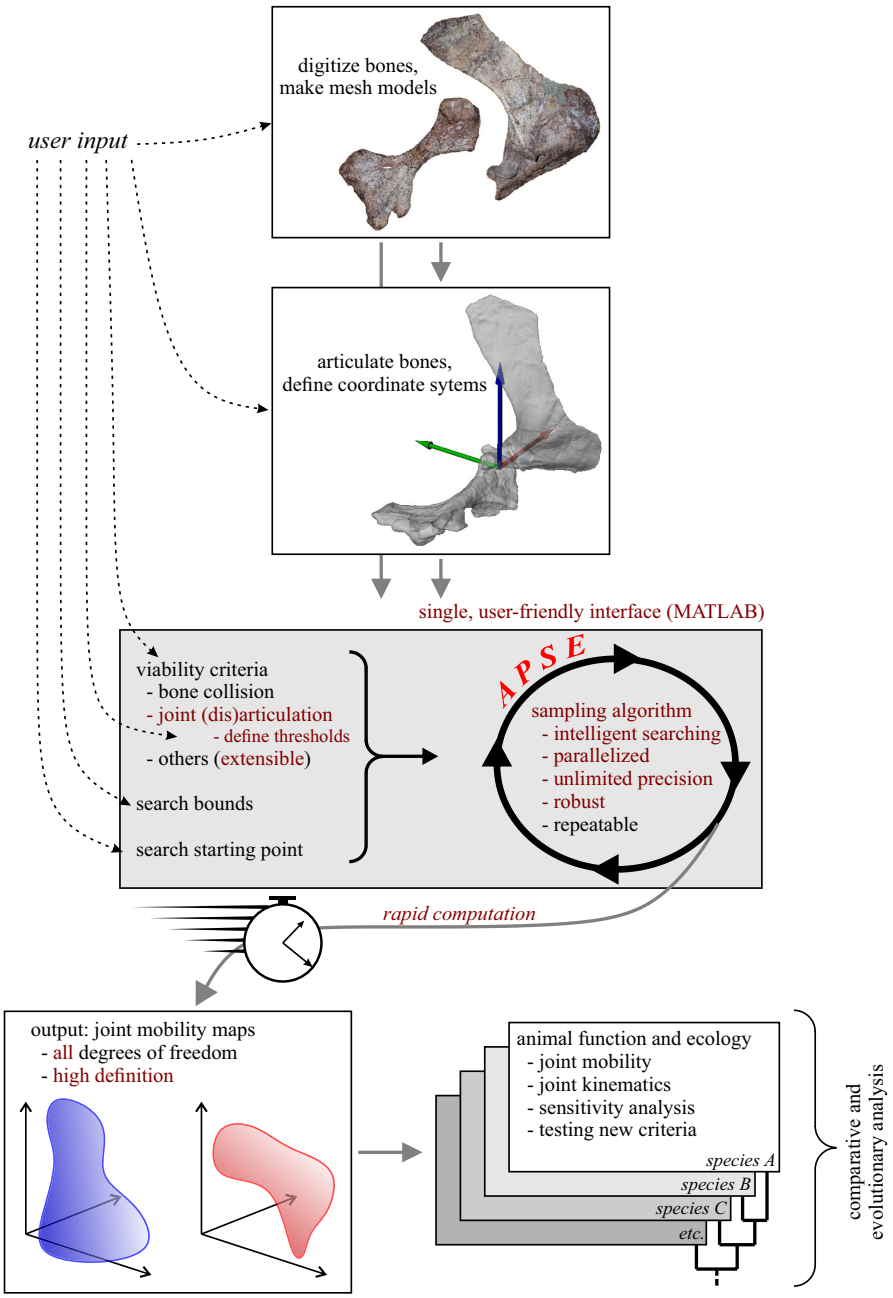

FIGURE 1 Schematic overview of the user workflow implementing the APSE algorithm in studies of joint mobility, outlining required data sources and input, and resulting outputs and potential downstream analyses. Key new additions or improvements over prior approaches are highlighted in red.

single generation (see Supporting Information). APSE terminates the search when either the maximum allowed number of generations has been reached, or when the envelope circumscribing viable parts of pose space ceases to grow significantly, whichever occurs first.

APSE was implemented in MATLAB (v9.5; MathWorks, Inc.), which offered at least three advantages over other methods or computing environments. First, it facilitated the detection of bone–bone mesh collision via the ray–triangle intersection algorithm of Möller and Trumbore (1997), obviating the need to generate a Boolean object as per current methods (Brocklehurst et al., 2022; Jones, Brocklehurst, et al., 2021; Manafzadeh & Gatesy, 2022; Manafzadeh & Padian, 2018), saving time. Second, the algorithm of Möller and Trumbore (1997) is indifferent to mesh manifoldness, and thus robust to mesh quality. Third, the MATLAB Parallel Computing Toolbox provides a substantial speed increase by executing multiple viability checks simultaneously, typically producing a four-fold or greater decrease in wall-clock time. Exhaustive sampling methods can also take advantage of parallelization (see below), but this is apparently not used in current methods.

2.2 | Illustrative tests

APSE has been extensively tested on a wide diversity of amniote fore- and hindlimb joint morphologies, but a select number of test cases are presented here for illustrative purposes. All tests were performed using a laptop computer with a 2.6 GHz processor (i9-11950H, 8 cores; Intel, USA).

2.2.1 | Geometric example

The algorithm's efficacy is first demonstrated using a 6 DOF, abstract geometric system comprising an inner and outer screw thread (Figure 2). Parameter settings used are reported in Table S1. Here, translations and rotations are very tightly coupled with one another, and this coupling can be analytically derived, irrespective of the coordinate system used (Supporting Information). The geometries of inner and outer threads were created in Rhinoceros (v4.0, McNeel), with a small spacing (1.46 mm) between the two. Without spacing, only a single path of rotations and translations would be permissible, producing pure helical motion; the spacing permits a small amount of 'wiggle room' (variation about the theoretical path). Even with such variation, tight coupling between rotations and translations would necessitate a very dense sampling with an exhaustive search (fine resolution sampling increment, e.g. sampling every 1°). Although a screw system is quite removed from the biological reality that end users of APSE would typically investigate, the purpose of this test is to demonstrate the potential precision that can be achieved, in comparison to a theoretically known result.

2.2.2 | Biological examples

Tests for three biological joint systems are illustrated here (Figure S3): a chicken hip (*Gallus gallus*; Bishop, Hocknull, Clemente, Hutchinson, Barrett, et al., 2018), a 'ball-and-socket' joint that is relatively unconstrained in rotational mobility; a human knee (*Homo sapiens*; Bishop, Hocknull, Clemente, Hutchinson, Farke, et al., 2018), a 'hinge-like' joint that is more constrained in its mobility; and the elbow (humeroulnar joint) of the extinct marsupial *Palorchestes azael*, whose mobility has been inferred to be highly constrained (Richards et al., 2021). Both the human knee and *Palorchestes* elbow are known or inferred to exhibit strong coupling of rotational and translational DOFs (Hirschmann & Müller, 2015; Richards et al., 2021). Mobility was measured in both 3 and 6 DOFs for each system. In the 3-DOF case, three approaches were used: (1) the current state-of-the-art for exhaustive sampling as implemented in Maya (v2022, Autodesk); (2) exhaustive sampling as implemented in MATLAB, leveraging parallelization and (3) APSE, also in MATLAB. In the 6-DOF case only, the two MATLAB implementations were tested. The parameter settings used are reported in Table S1; a higher value of k was used for the biological examples compared to the screw example due to the expected tight coupling between DOFs in the screw (reducing the frequency of 'inviability overshoot'; see Supporting Information). The purpose of the biological tests was to (1) evaluate the equivalence of results between Maya- and MATLAB-based implementations of an exhaustive search and (2) evaluate the efficiency of APSE in comparison to the MALTAB-based exhaustive search. As APSE involves a stochastic element, repeatability of results was assessed by running each test 10 times. For comparisons involving the volumes of viable mobility space, volumes were computed by 'shrink wrapping' polygonal alpha shapes to the (cosine-corrected) data, with a radius equal to the critical radius or 10 (for rotations) or 1 (for translations), whichever was greater (Manafzadeh & Gatesy, 2020). Volumes or subsets thereof were computed in CloudCompare (v2.11.3, http://cloudcompare.org/) and MeshLab (v 1.3.3, http://meshlab.sourceforge.net/).

In the 3-DOF tests, pose viability was assessed only against the criterion of bone–bone collision. In 6-DOF analyses, using just this criterion is not sensible without prior knowledge of the achievable limits to translation, as might be informed from in vivo or ex vivo data (Manafzadeh & Gatesy, 2021); without such limits, the translational component of viable pose space is essentially unconstrained (box-like mobility envelope), and in turn so too is the rotational component of viable pose space. Thus, a second criterion was implemented, using the amount of overlap of apposing articular surfaces as a measure of joint disarticulation (see Supporting Information), where <50% overlap has generally been taken to indicate disarticulation (Brocklehurst et al., 2022; Jones, Brocklehurst, et al., 2021; Kambic, Biewener, et al., 2017; Lai et al., 2018; Molnar et al., 2021; Pierce et al., 2012; Stevens & Parrish, 1999). It must be

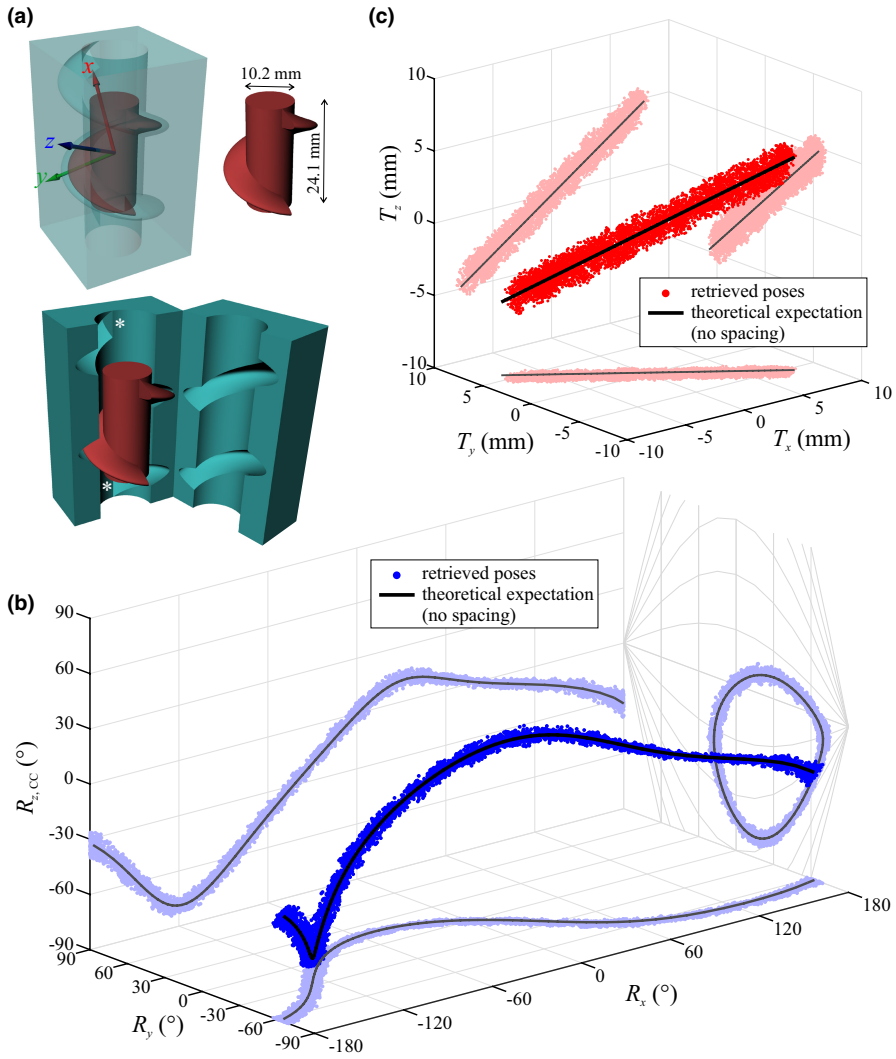

FIGURE 2 Test of APSE's efficacy using an abstract system whose rotational and translational mobility are both highly constrained and theoretically known a priori. (a) The geometry involved, comprising an inner (maroon) and outer (turquoise) screw thread, with stops at either end (*) to limit the amount of along-axis rotation and translation. The coordinate system axes are randomly rotated; the exact orientation is inconsequential. (b, c) Comparison of recovered viable poses plotted in cosine-corrected rotational (b) and translational (c) mobility space, with theoretically expected rotations and translations superimposed. The algorithm successfully and densely (15,416 coordinates) captures the tight coupling of rotational and translational mobility across the full range of motion.

emphasized that 'overlap' is at present an ill-defined term whose biological or physical relevance remains to be evaluated in detail (see Kambic, Biewener, et al., 2017), although the present study offers a starting point.

2.3 | Application: 'Pelycosaur' shoulders

As a case study, APSE was used to explore mobility of the shoulder of 'pelycosaur'-grade synapsids. Along with other early amniotes (e.g. Fox & Bowman, 1966; Holmes, 1977) and some temnospondyls (e.g. Miner, 1925), the pelycosaurian shoulder joint exhibits an enigmatic morphology, comprising a 'screw-shaped' glenoid and a strap-like caput that spirals about the terminal end of the proximal humerus (Figure 3a,b). Apposing joint surfaces are highly congruent, suggestive of minimal articular cartilage (Bonnan et al., 2013). Rather than being a peculiar evolutionary tangent, this morphology is a key component to the history of vertebrate terrestrialization: it appears to have evolved convergently in both stem-amniotes and temnospondyls, in association with convergent acquisition of a 'twisted' or 'tetrahedral' humerus (Dickson et al., 2020), and was therefore ancestral for all extant tetrapod clades. Due to its importance, the function and adaptive significance of this anatomy has long been debated (Fox & Bowman, 1966; Haines, 1952; Holmes, 1977; Jenkins Jr., 1971; Miner, 1925; Romer, 1922; Watson, 1917). Previous studies concur that shoulder movement in animals with this morphology was highly stereotyped, with the power stroke (~stance phase) involving a combination of humeral retraction, pronation (internal rotation) and glenohumeral sliding. Yet, this hypothesis remains to be quantitatively tested, and the function of the joint during the recovery stroke (~swing phase) has been comparatively neglected.

To provide new perspective, this study focused on *Dimetrodon*, an iconic genus from the early Permian of the USA and Germany (~280 Ma; Romer & Price, 1940) that has played a central role in studies examining the evolution of locomotor function in synapsids (Haines, 1952; Hopson, 2015; Jenkins Jr., 1971, 1973; Jones, Dickson, et al., 2021; Romer, 1922; Watson, 1917). Three excellently preserved, associated specimens were used; two of *D. milleri* and one of *D. limbatus* (Table S2). Models of the scapulocoracoid and humerus of specimen MCZ VPRA-1365 were generated by micro-computed tomographic scanning (X-Tek HMXST225, Nikon Metrology, U.K.; 130 kV and 165 μA with 0.5 mm copper filter; voxel

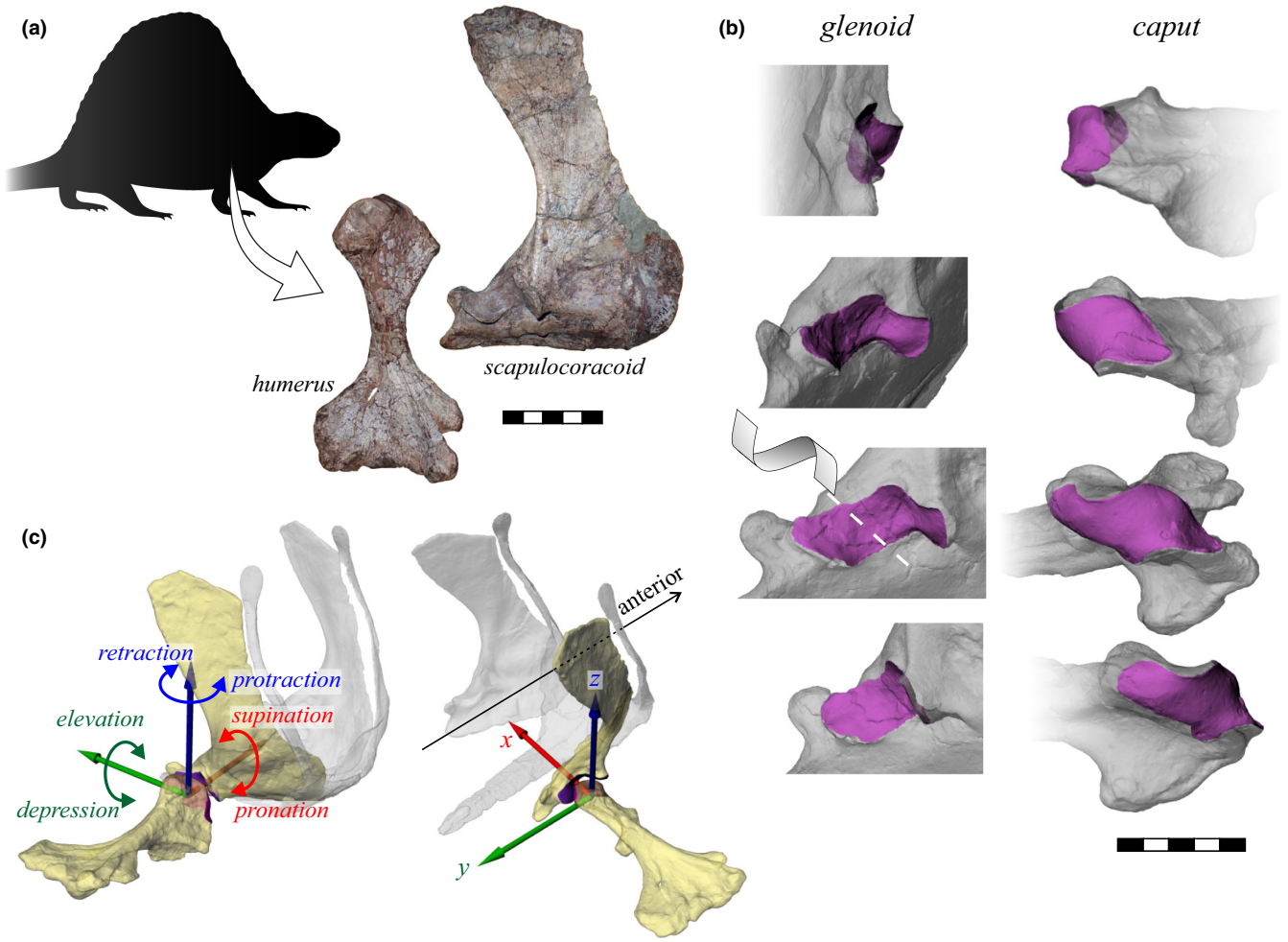

FIGURE 3 Analysing mobility in the enigmatic shoulder joint of 'pelycosaurs'. (a) This study focused on two species of *Dimetrodon*, with the left scapulocoracoid and humerus (both reversed) of MCZ VPRA-1365 *D. milleri* shown here. (b) Close-ups on the right scapulocoracoid glenoid and humeral caput of a digital rendering of MCZ VPRA-3357 *D. limbatus*, shown in four views successively rotated about the vertical axis by 45° (third row is pure lateral view); articular surfaces highlighted in purple. The humerus is mirrored (i.e. it appears as a left element) to show correspondence in articular surfaces between glenoid and caput. (c) Reference pose and joint coordinate system used for the right shoulder, shown in two oblique dorsolateral views. Scale bars in a and b are 50 mm.

resolution 0.127 [scapulocoracoid] and 0.074 [humerus] mm) and segmentation in Mimics (v22, Materialize, Belgium). Models of the scapulocoracoid and humerus of MCZ VPRA-1367 and VPRA-3357, and dermal girdle elements of VPRA-1365, were digitized by photogrammetry (RealityCapture v1.2, Epic Games, Slovakia). Bones were then assembled and oriented into a reference pose and joint coordinate system in Rhinoceros, following Brocklehurst et al. (2022) and Gatesy et al. (2022) (Figure 3c; Supporting Information). Shoulder orientation is described using an intrinsic Euler sequence of protraction–retraction (*z*-axis), followed by elevation–depression (*y*-axis), followed by long-axis rotation or pronation–supination (*x*-axis).

Sampling parameter settings used are reported in Table S2. More than any other 'pelycosaur'-grade genus, adult *Dimetrodon* limb elements are very well ossified, resulting in well-delineated and highly congruent articular surfaces. In MCZ VPRA-1365, the mesh separation threshold for disarticulation was estimated as 5 mm, based on visual assessment of the fossil material when physically articulated (Figure S4D–F); the threshold assigned for the other specimens was scaled from this by virtue of glenoid anteroposterior diameter. High joint congruence suggests that a large amount of contact between apposing articular surfaces occurred in life (see aforementioned studies), so the mesh overlap threshold was assigned conservatively as 66.7%: at most, one-third of the humeral caput could be disarticulated in a given pose. To evaluate the sensitivity of sampling to this choice, the algorithm was re-run with an overlap threshold of 50%, which would be expected to increase potential mobility.

3 | RESULTS

3.1 | Screw example

The APSE algorithm converged in 3 h 9 min, taking 202 generations to retrieve 15,416 viable poses from a total of 100,976 samples (15.3% recovery rate). It captured the expected tight coupling between rotations and translations over the system's full range of

motion (Figure 2b,c). Were an exhaustive sampling approach used, a very fine rotational and translational increment would be needed to approach the same density of sampling (and therefore detail), requiring a prohibitively long computation time. For instance, even at a coarse resolution increment of 5° and 1 mm (>1.13×10^9 combinations) and generously assuming that 100 poses s^{-1} could be evaluated, this would still take >130 days to complete.

3.2 | Biological examples

Results for the 3- and 6-DOF tests are shown in Figures 4 and 5, respectively. Results for the MATLAB implementation of an exhaustive search were equivalent to those for the state-of-the-art Maya implementation, with an identical set of viable poses retrieved and recovery rate (Figure 4d,e). The MATLAB exhaustive search also took considerably less time to execute (Figure 4c). The APSE algorithm exhibited stereotyped convergence behaviour, involving a sigmoidal time history to alpha shape volume growth (Figure 4b): exploration of pose space was initially accelerated by electrostatic repulsion, followed by saturation of viable poses and slowing down in later generations. APSE retrieved a far greater number of viable poses compared to exhaustive sampling (Figures 4d and 5d), with a much higher recovery rate (Figures 4e and 5e). The resulting mobility envelopes were generally more extensive, more densely sampled and had greater definition compared to those produced by exhaustive sampling (see also Figure S5). In 3-DOF tests, the time taken by APSE compared to the exhaustive search varied; tests that involved more combinations of rotations to evaluate exhaustively were more efficiently sampled than tests that involved fewer combinations (compare chicken v. *Palorchestes*; Figure 4c and Table S1). Thus, when more DOFs are involved, increasing the number of potential poses, the intelligent sampling of APSE was emphatically faster (Figure 5c).

When measured in terms of the volume of overlap between mobility envelopes, APSE also captured a very high proportion (rotations: 86.7%–99.9%, mean 95.6%; translations: 81.4%–99.7%, mean 89.0%) of viable poses identified by exhaustive sampling (Figures 4f and 5f), and indeed captured parts of viable mobility space not recovered by exhaustive sampling, due to the latter's fixed sampling resolution. That is, for a given amount of wall-clock time, APSE has the potential to achieve greater fidelity with respect to the result of an infinitely dense or long search, and in turn can more reliably capture a greater portion of those poses that are viable (see also Supporting Information). Poses identified by exhaustive sampling that were not captured by APSE tended to lie just beyond the latter's resulting mobility envelope (yellow points in Figures 4a and 5a,b). These points are instances of non-sampling, rather than false negatives, whereby continued running of the algorithm (i.e. use of stricter convergence criteria) would eventually capture them. The aforementioned results involve small to very small variability, indicating a high level of repeatability to the results obtained via APSE (see also Table S3). Although not illustrated here, additional testing demonstrated that results are robust to variation in the initial seed point used, although convergence time can vary.

3.3 | *Dimetrodon* shoulder

Results for MCZ VPRA-1365 *D. milleri* are reported here; those obtained for the other specimens were highly similar and are illustrated in Figures S6 and S7. With a 66.7% overlap threshold, the mobility map of viable rotations forms a distinctive tetrahedral shape in cosine-corrected space; in Figure 6a, the edges of this tetrahedron are delimited by exemplar poses 1–3 and 6–8. Due to this shape, all three rotational DOFs are coupled with one another, and moreover the coupling at high levels of depression (pronation-with-retraction) is reversed at high levels of elevation (supination-with-retraction). Intermediate levels of depression permit a small but significant amount of variability in achievable poses (poses 4, 5). Translational mobility also exhibits marked coupling (Figure 6b). This is particularly apparent between translations in the *y*- and *z*-directions, where movement is back-and-up or forward-and-down, essentially parallel to the axis of an imaginary screw describing the glenoid surface (cf. Figure 6b). Coupling also occurs between translations and all rotational DOFs, particularly elevation–depression (R_y), although this is not strictly monotonic across the full range of motion. These fundamental patterns remain unaltered when the 50% overlap threshold is used (Figures S6 and S7); viable mobility space essentially remains the same shape, but is expanded to encompass a greater variety of achievable poses.

4 | DISCUSSION

4.1 | APSE: An improved algorithm

A key shortcoming of current approaches for digital investigation of joint mobility is the large computing time required by exhaustive search methods to delimit viable parts of pose space (Manafzadeh & Gatesy, 2022). The intelligent algorithm implemented in APSE addresses this issue, generating a high-definition mobility map of viable joint poses in substantially less time. Yet, the resulting mobility map has a similar (often better) coverage of viable pose space compared to that achieved by exhaustive sampling. APSE greatly reduces the time spent evaluating inviable regions of pose space, with recovery rates orders of magnitude higher than an exhaustive search; fewer poses need to be evaluated to achieve the same level of mobility map detail. This ultimately results in more viable poses being retrieved, and a higher precision assessment of rotational and translational mobility. As more DOFs are considered, the number of possible poses to evaluate grows exponentially, such that the computational requirement of an exhaustive search quickly becomes intractable. However, the proportion of these poses that are inviable will remain high (potentially even increasing), such that the time saved by avoiding inviable regions

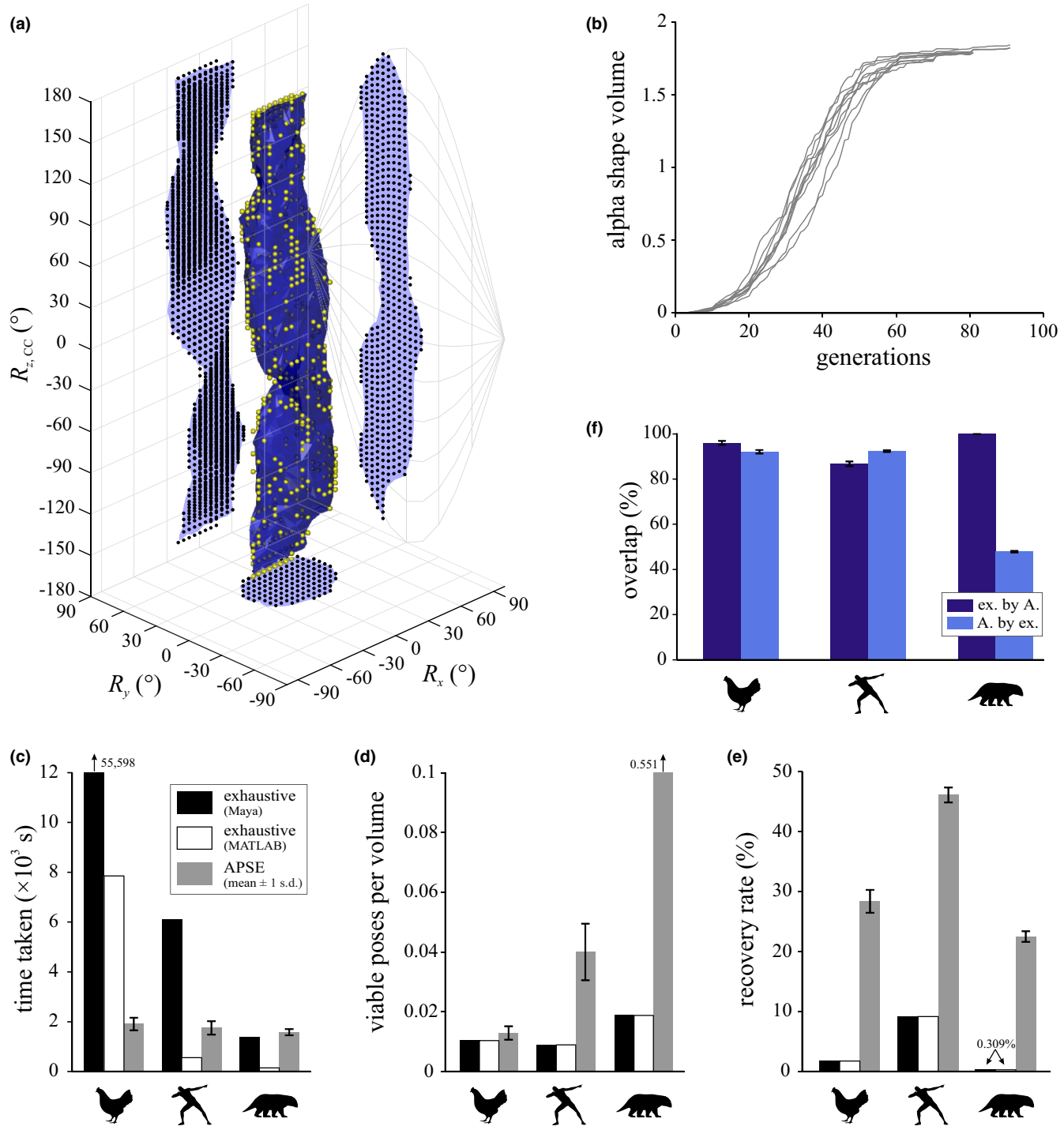

FIGURE 4 Results for three degree of freedom (rotations only) testing of the biological joints. (a) Exemplar results plotted in cosine-corrected mobility space, here for the chicken hip. Blue denotes the region of viable poses retrieved by APSE, with black points denoting (the projections of) viable poses identified by exhaustive sampling. Yellow points denote viable poses identified by the exhaustive sampling that were not captured by APSE (i.e. do not fall within alpha shape). (b) Exemplar convergence trajectories for APSE, here for the human knee; note that the absolute magnitude of alpha shape volume is meaningless as it is calculated in scaled design space (see Supporting Information). (c–e) Comparison of results between exhaustive sampling Maya implementation, exhaustive sampling MATLAB implementation and APSE, in terms of time taken (c), number of viable poses retrieved per unit volume of the mobility envelope (poses per cubic degree, d) and recovery rate (e, i.e. number of viable poses retrieved relative to total number of poses sampled). (f) Comparison of amount of reciprocal overlap in viable poses retrieved between exhaustive ('ex.') and APSE ('A.') approaches, in terms of shared alpha shape volumes.

of pose space will also grow exponentially: the efficiency of the algorithm is expected to remain relatively unaffected by the number of DOFs.

The underlying reasons for the improvements offered by APSE and its present implementation are manifold. Increased algorithm speed is due to mechanisms that preferentially target

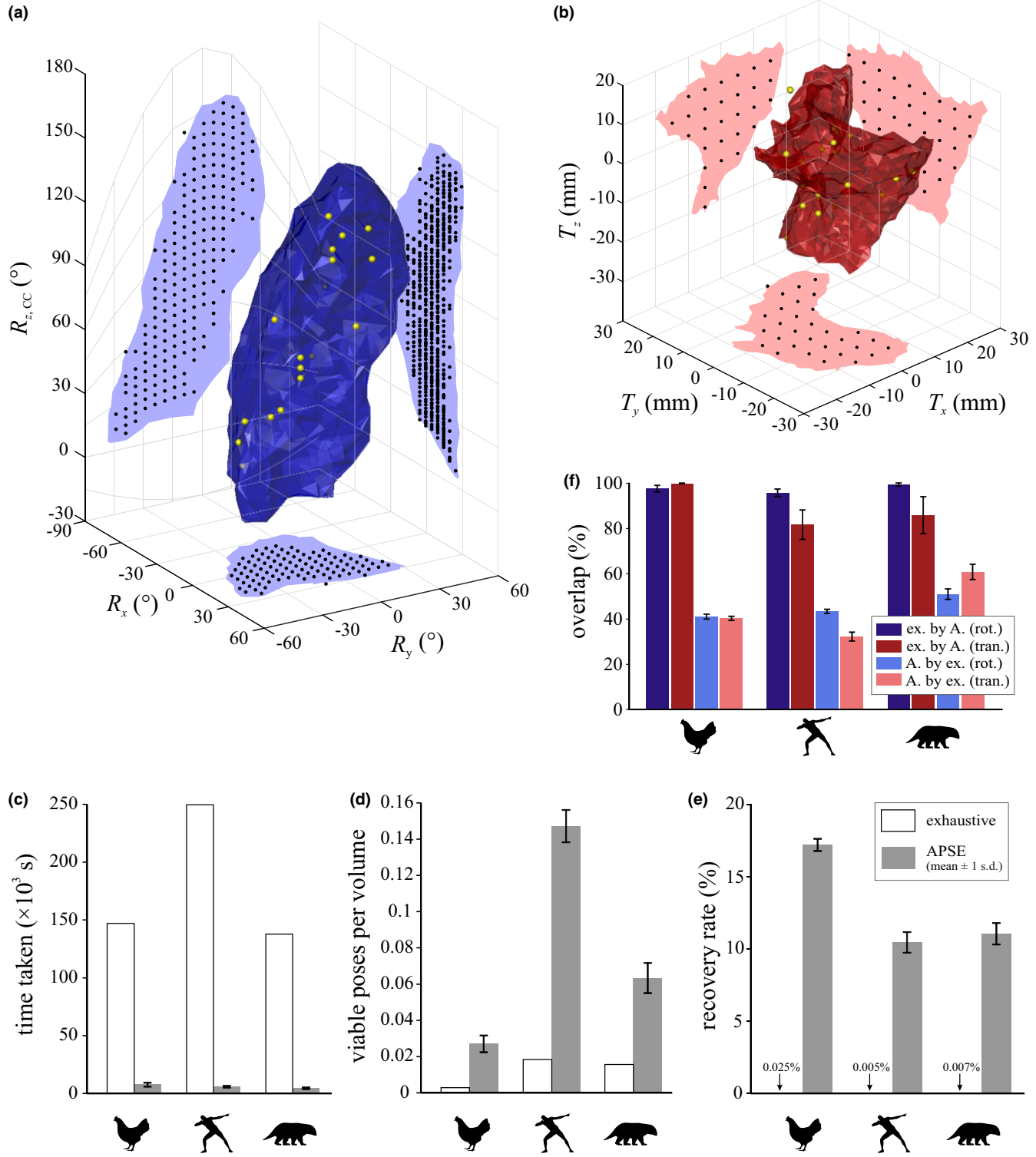

FIGURE 5 Results for six degree of freedom testing of the biological joints. (a, b) Exemplar results plotted in cosine-corrected rotational (a) and translational (b) mobility space, here for the *Palorchestes* elbow. Blue and red denote the region of rotational (blue) and translational (red) components of viable poses retrieved by APSE; other conventions as per Figure 4. (c–e) Comparison of results between exhaustive search (MATLAB implementation) and APSE, in terms of time taken (c), number of viable poses retrieved per unit volume of the rotational mobility envelope (d) and recovery rate (e). (f) Comparison of amount of reciprocal overlap in viable poses retrieved between exhaustive ('ex.') and APSE ('A.') approaches, for rotational ('rot.') and translational ('tran.') components.

under-sampled regions of pose space and avoid already sampled regions of pose space; this includes both the selection of regions of pose space for seeding the next generation of particles, and the use of electrostatic repulsion. In the latter, the current generation of particles 'remembers' where other generations of particles have previously been, helping to drive new generations of particles out

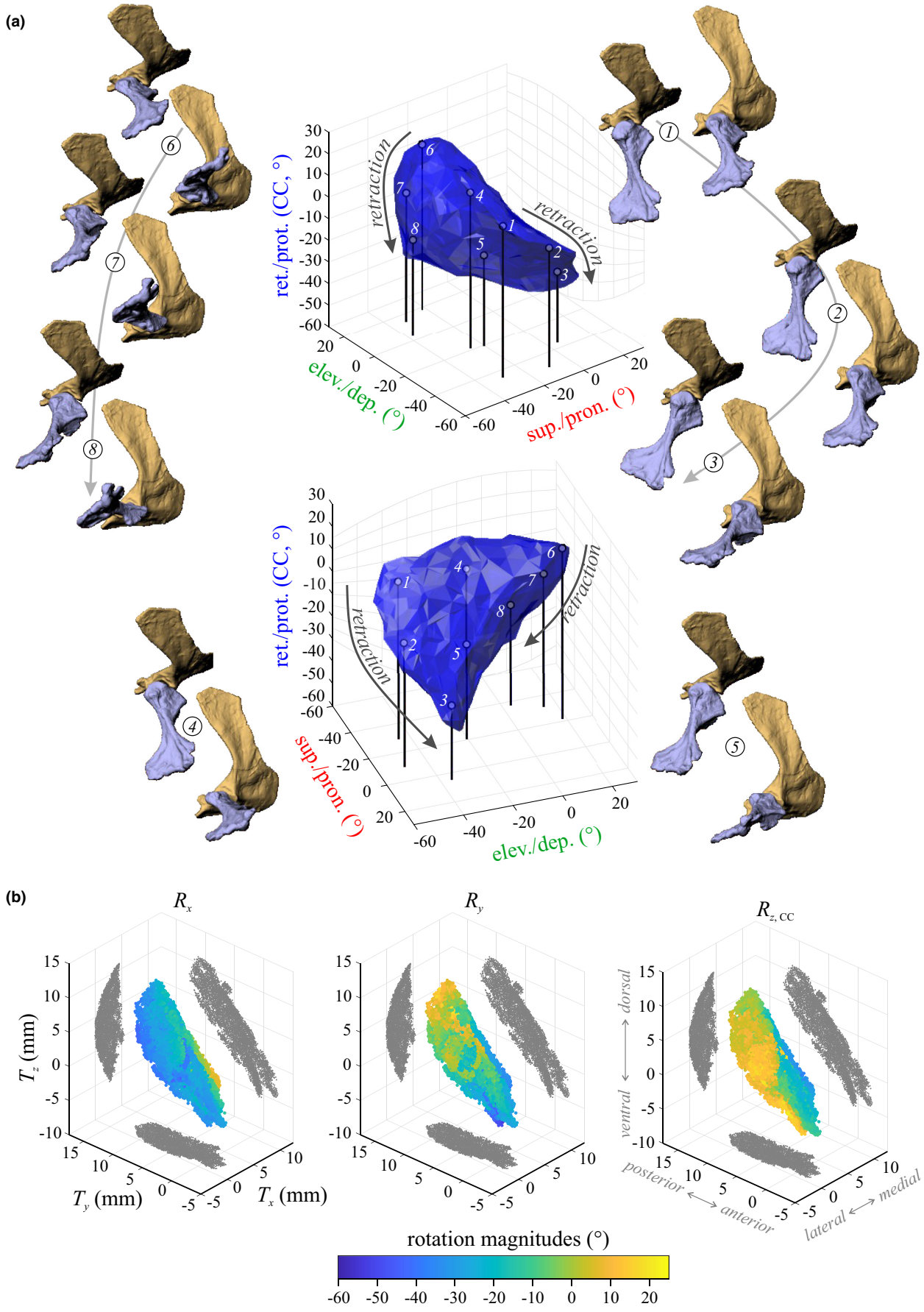

FIGURE 6 Shoulder mobility recovered for MCZ VPRA-1365 *D. milleri* using the 66.7% overlap threshold. (a) Cosine-corrected rotational mobility, with several examples throughout viable pose space to illustrate variation in achievable poses, shown in lateral and dorsolateral views of the right side. Poses 1–3 and 6–8 illustrate coupling between degrees of freedom (DOFs) that occurs at low and high elevation angles, respectively. (b) Translational mobility, with individual poses colour-coded by the corresponding values of rotational DOFs. Collectively, shoulder mobility in *Dimetrodon* is characterized by marked coupling between both rotations and translations across its range of motion.

into unexplored pose space. Additional substantial improvements to speed are gained from the parallelization of pose viability evaluation, and more efficient detection of bone–bone collisions (Möller & Trumbore, 1997), the latter of which is also robust to mesh quality (manifoldness). Furthermore, the Brownian motion and electrostatic repulsion components of the algorithm enable particles to explore pose space at a precision limited by the floating-point precision of the computer used, typically on the order of 10^{-16}. This offers the potential for much greater definition to the surface of a mobility envelope than could be achieved via (exhaustive) sampling at fixed increments, and enables APSE to detect viable combinations of rotations and translations that are simply never queried by exhaustive sampling, due to the latter's fixed sampling resolution (see Supporting Information). One final advantage offered by APSE is that new generations of particles remain spatially connected with their predecessors, and hence it will not falsely retrieve 'islands' of viable pose space that are detached from the main mobility envelope (e.g. Brocklehurst et al., 2022; Demuth et al., 2020). Although such islands may be viable according to the criteria implemented, they are biologically implausible because real joints cannot 'teleport' across a span of inviable pose space. Moreover, in some situations, these islands are ostensibly erroneous (e.g. bones upside down; see Regnault & Pierce, 2018).

4.2 | Aspects for future improvement

Despite the advantages offered by APSE, it is not without limitations, which should be borne in mind. For instance, it requires the user to provide an initial pose as the seed point from which to commence the search, one that must be viable. If multiple, complex viability criteria are involved, the determination of such a pose may become difficult and time-consuming if undertaken manually. Potentially, automated derivation of viable seed poses in future studies may be assisted through the calculation of joint-centric 'anatomically neutral poses' (e.g. Brocklehurst et al., 2022). Variation in the chosen seed point may also increase the potential for variation (stochasticity) in the results; although the resulting mobility envelope may remain grossly unaffected, time to convergence and the number of viable poses retrieved may differ significantly.

More broadly, APSE is designed to elucidate the *envelope* of joint rotational and translational mobility. It is therefore well-suited if the investigator's interest lies in the geometry of the periphery of viable pose space, that is, the mobility map and limits to joint excursion. By contrast, while the interior of viable pose space is densely sampled here—more so than achieved with exhaustive sampling—this sampling is not regular or uniform (Figure S5), which may not be appropriate for analyses that require such sampling (e.g. investigating how articulation itself changes throughout joint movement). In these cases, a fixed-increment exhaustive search would be required, although it should be noted that even then the resulting sample may not be uniform in directional terms (Manafzadeh & Gatesy, 2020; Pataky & Challis, 2020).

One further point worth emphasizing is that, in and of itself, APSE does not provide any progress on achieving more 'biologically realistic' results, such as how well a recovered mobility map reflects the limits to joint excursion measured in ex vivo (Manafzadeh, 2020; Regnault et al., 2021) or in vivo (Kambic, Roberts, et al., 2017) experiments. Importantly, however, the rapidity of the algorithm allows for inclusion of all 6 DOFs and the checking of multiple viability criteria to be layered onto one another without substantial increases to computational load: assessing fewer poses more quickly enables more time to be dedicated towards evaluating viability for each pose. Achieving greater biological realism is contingent on the use of more empirically benchmarked viability criteria, which requires much future scrutiny (Manafzadeh & Gatesy, 2022). Moving forwards, the choice and implementation of viability criteria for generating biologically realistic mobility maps therefore remains the responsibility of the investigator. To that end, the present study employed two basic criteria that have been used by numerous previous studies (bone–bone collision and joint disarticulation), which serve to achieve a constrained mobility map. However, the biological significance of the map geometry recovered needs to be interpreted holistically, using multiple lines of evidence.

4.3 | 'Pelycosaur' shoulder function

Investigation of shoulder mobility in *Dimetrodon* using APSE shows that the glenohumeral joint is characterized by marked coupling between almost all rotational and translational DOFs across its range of motion. Coupled rotations and translations have previously been inferred for the screw-shaped glenoid, in particular humeral pronation and anteroposterior sliding in tandem with retraction during the power stroke (Fox & Bowman, 1966; Holmes, 1977; Jenkins Jr., 1971; Miner, 1925; Watson, 1917). The present study provides the first quantitative support of this hypothesis.

The ubiquity of the screw-shaped glenoid among early amniotes and temnospondyls suggests that the pattern recovered here for *Dimetrodon* likely applies to many other taxa as well. However, almost all previous studies have considered shoulder function

during the power stroke only, ignoring motions during the recovery stroke (humeral protraction). Watson (1917) inferred highly stereotyped mobility in *Dimetrodon*, suggesting that recovery stroke was essentially power stroke played in reverse. Arguing against this, the 66.7% overlap results show that some potential for pose variability remains at intermediate levels of depression (around −20°; Figure 6a, poses 4, 5); recovery and power strokes could have followed different trajectories through pose space. Using a less conservative 50% overlap threshold would have permitted even greater mobility (Figures S6 and S7), further supporting this inference. (It is expected that using a larger separation threshold distance would have a similar effect.) This parallels the suggestions of Fox and Bowman (1966) and Holmes (1977), who hypothesized a division of labour between different parts of the shoulder joint surfaces in captorhinids, corresponding to different kinematics between power and recovery strokes. Yet, captorhinids possess a longitudinal ridge on the glenoid that is absent in 'pelycosaurs' and temnospondyls (Holmes, 1977, fig. 7), so the interpretation of functional division of labour may not generalize to all taxa.

The marked coupling between rotational DOFs in the *Dimetrodon* shoulder highlights a potential functional explanation for its bizarre anatomy, one that is absent among extant tetrapods. Progressive pronation in tandem with retraction, especially at more depressed poses, is the same fundamental kinematic pattern observed in the shoulder of extant sprawling tetrapods during locomotion (e.g. Nyakatura et al., 2019). Extant taxa typically possess a relatively simplistic shoulder morphology (Jenkins Jr., 1993; Miner, 1925; Walker, 1973), whereby movements must be principally coordinated by neuromuscular control ('soft' mechanisms). In contrast, these movements in *Dimetrodon*, and likely many early amniotes and temnospondyls, appear to have been guided automatically from the bony anatomy ('hard' mechanisms). Previously, Jenkins Jr. (1971) suggested that reliance on structural regulation to prescribe joint movement implied compensation for a lowered capacity for complex neuromuscular coordination as these animals were still evolving terrestrial proficiency. However, in vivo studies indicate broad conservatism in neuromuscular control across extant tetrapods (Jenkins Jr. & Goslow Jr., 1983; Peters & Goslow Jr., 1983; Pierce et al., 2020), suggesting that the fundamental components were already present in the last common ancestor of crown tetrapods. The adaptive value of the screw-shaped glenoid may alternatively lie in conferring reductions in locomotor costs: greater control of joint motion by hard mechanisms could reduce the muscular effort required for limb positioning and antigravity support, in turn reducing energetic expenditure. Greater osteological regulation of joint motion could also compensate for weaker muscles (by contributing more to joint moment balance) or less stereotyped muscular control, in the latter case acting as a physical 'diode' that accommodated greater variability in applied muscular forces to still produce desirable joint motion. In this scenario, the screw-shaped glenoid may be thought of as a transient solution to the problem of weight support and movement in a fully terrestrial animal, building upon an already partly constrained glenohumeral anatomy in the earliest tetrapods (Pierce et al., 2012). Emphasis in joint control subsequently shifted more to soft mechanisms in more derived Permo-Triassic taxa (e.g. therapsids), presumably as greater postural and behavioural flexibility became of greater importance.

5 | CONCLUSIONS

APSE provides a novel approach for more rapid and more precise sampling and circumscription of high-dimensional joint mobility space. Leveraging parallel computing and mechanisms for targeting under-explored regions of pose space, APSE attains computational speeds and recovery rates orders of magnitude greater than state-of-the-art exhaustive approaches. Rapid and robust quantitative implementations of viability criteria evaluation are also included in the algorithm. The application of APSE has been illustrated here in 6 DOFs, but it is mathematically scalable to any number of dimensions in the future. Collectively, these advancements greatly lower the barrier to researchers seeking to investigate joint function, particularly in complex systems where more dimensions or pose viability criteria are involved, accelerating the pace of research in comparative or evolutionary analyses of animal function.

Looking forward, APSE opens up new opportunities for more efficiently exploring the movements and interactions of several bones in complex vertebrate joints, such as the humerus, radius and ulna in the elbow (Hutson & Hutson, 2015; Landsmeer, 1983) or the tarsals of the pes (Turner & Gatesy, 2021), which have generally proven intractable for detailed quantitative analysis as there can be up to 6 DOFs per bone involved. In addition, providing a more detailed, quantitative view of the interactions between rotational and translational DOFs within joints will facilitate the development of more sophisticated computational models of the musculoskeletal system. Incorporating translations as functions of rotations (e.g. Yamaguchi & Zajac, 1989), or vice versa, can better integrate joint complexity with musculoskeletal modelling methods, which currently rely heavily on minimalistic rotational joints (Bishop et al., 2021; Brocklehurst et al., 2022; Maidment et al., 2014; Molnar et al., 2021; Regnault et al., 2021). The greater unification of these disparate datasets and approaches can be reciprocally illuminating, helping to improve understanding of animal musculoskeletal anatomy, function, behaviour and ecology throughout evolutionary history.

AUTHOR CONTRIBUTIONS

Peter J. Bishop conceived the original gross structure of the algorithm; Peter J. Bishop and Robert J. Brockehurst refined and tested the algorithm in its final form; all authors contributed to study design, results interpretation and manuscript writing.

ACKNOWLEDGEMENTS

S. Regnault is thanked for undertaking tomographic scanning of MCZ VPRA-1365; C. Byrd is thanked for assistance with access to fossil material; S. Gatesy, E. Herbst, A. Krahl, J. van Beesel and an anonymous reviewer are thanked for constructive and thoughtful criticisms of earlier versions of the manuscript. This work was supported by the William F. Milton Fund (Harvard University, to

S.E.P.) and United States National Science Foundation grants DEB-1754459 and EAR-2122115 (to S.E.P.). Lastly, apses are large polygonal (or semicircular) voids to be found in churches; the name of the new algorithm was inspired by this fact, and pays homage to the authors' predecessors who were similarly influenced by ecclesiastical architecture (Gould & Lewontin, 1979).

CONFLICT OF INTEREST

The authors declare no conflict of interest.

PEER REVIEW

The peer review history for this article is available at https://publons.com/publon/10.1111/2041-210X.14016.

DATA AVAILABILITY STATEMENT

A complete set of code, including a graphical interface, for running both APSE and exhaustive (parallelized) sampling algorithms in MATLAB are available through Harvard's Dataverse Repository at https://doi.org/10.7910/DVN/G0SHOQ (Bishop et al., 2022a). The full set of code and data required to reproduce the results reported here are also included in this repository. Fossil *Dimetrodon* specimens are held in the Vertebrate Palaeontology (Reptiles and Amphibians) collection of the Museum of Comparative Zoology, Harvard University; digital models of the specimens are available through MorphoSource at www.morphosource.org/projects/000473811 (Bishop et al., 2022b). All imagery of specimens is copyright of the President and Fellows of Harvard University.

ORCID

Peter J. Bishop https://orcid.org/0000-0003-2702-0557
Robert J. Brocklehurst https://orcid.org/0000-0002-3017-6838
Stephanie E. Pierce https://orcid.org/0000-0003-0717-1841

REFERENCES

Béchard, I., Arsenault, F., Cloutier, R., & Kerr, J. (2014). The Devonian placoderm fish *Bothriolepis canadensis* revisited with three-dimensional digital imagery. *Palaeontologia Electronica*, *17*, 2A.

Bicknell, R. D. C., Melzer, R. R., & Schmidt, M. (2022). Three-dimensional kinematics of euchelicerate limbs uncover functional specialization in eurypterid appendages. *Biological Journal of the Linnean Society*, *135*, 174–183.

Bishop, P. J., Brocklehurst, R. J., & Pierce, S. E. (2022a). Supporting information for: Intelligent sampling of high-dimensional joint mobility space for analysis of articular function. *Harvard Dataverse*. https://doi.org/10.7910/DVN/G0SHOQ

Bishop, P. J., Brocklehurst, R. J., & Pierce, S. E. (2022b). Data from: Intelligent sampling of high-dimensional joint mobility space for analysis of articular function. *MorphoSource*. www.morphosource.org/projects/000473811

Bishop, P. J., Cuff, A. R., & Hutchinson, J. R. (2021). How to build a dinosaur: Musculoskeletal modelling and simulation of locomotor biomechanics in extinct animals. *Paleobiology*, *47*, 1–38.

Bishop, P. J., Hocknull, S. A., Clemente, C. J., Hutchinson, J. R., Barrett, R. S., & Lloyd, D. G. (2018). Cancellous bone architecture and theropod dinosaur locomotion. Part II – A new approach to reconstructing posture and locomotor biomechanics in extinct tetrapod vertebrates. *PeerJ*, *6*, e5779.

Bishop, P. J., Hocknull, S. A., Clemente, C. J., Hutchinson, J. R., Farke, A. A., Beck, B. R., Barrett, R. S., & Lloyd, D. G. (2018). Cancellous bone architecture and theropod dinosaur locomotion. Part I – An examination of cancellous bone architecture in the hindlimb bones of theropods. *PeerJ*, *6*, e5778.

Bonaparte, J. F. (1984). Locomotion in rauisuchid thecodonts. *Journal of Vertebrate Paleontology*, *3*, 210–218.

Bonnan, M. F., Wilhite, D. R., Masters, S. L., Yates, A. M., Gardner, C. K., & Aguiar, A. (2013). What lies beneath: Sub-articular long bone shape scaling in eutherian mammals and saurischian dinosaurs suggests different locomotor adaptations for gigantism. *PLoS ONE*, *8*, e75216.

Brocklehurst, R. J., Fahn-Lai, P., Regnault, S., & Pierce, S. E. (2022). Musculoskeletal modeling of sprawling and parasagittal forelimbs provides insight into synapsid postural transition. *iScience*, *25*, 103578.

Clark, E. G., Hutchinson, J. R., Bishop, P. J., & Briggs, D. E. G. (2020). Arm waving in stylophoran echinoderms: Three-dimensional mobility analysis illuminates cornute locomotion. *Royal Society Open Science*, *7*, 200191.

Demuth, O. E., Rayfield, E. J., & Hutchinson, J. R. (2020). 3D hindlimb biomechanics of the stem-archosaur *Euparkeria capensis* with implications for postural evolution within Archosauria. *Scientific Reports*, *10*, 15357.

Dickson, B. V., Clack, J. A., Smithson, T. R., & Pierce, S. E. (2020). Functional adaptive landscapes predict terrestrial capacity at the origin of limbs. *Nature*, *589*, 242–245.

Fox, R. C., & Bowman, M. C. (1966). Osteology and relationships of *Captorhinus aguti* (cope) (Reptilia: Captorhinomorpha). *The University of Kansas Paleontological Contributions*, *Vertebrata*, *11*, 1–79.

Gatesy, S. M., & Baier, D. B. (2005). The origin of the avian flight stroke: A kinematic and kinetic perspective. *Paleobiology*, *31*, 382–399.

Gatesy, S. M., Bäker, M., & Hutchinson, J. R. (2009). Constraint-based exclusion of limb poses for reconstructing theropod dinosaur locomotion. *Journal of Vertebrate Paleontology*, *29*, 535–544.

Gatesy, S. M., Manafzadeh, A. R., Bishop, P. J., Turner, M. L., Kambic, R. E., Cuff, A. R., & Hutchinson, J. R. (2022). A proposed standard for quantifying 3-D hindlimb poses in living and extinct archosaurs. *Journal of Anatomy*, *241*, 101–118.

Gould, S. J., & Lewontin, R. C. (1979). The spandrels of san Marco and the Panglossian paradigm: A critique of the adaptationist programme. *Proceedings of the Royal Society of London, Series B*, *205*, 581–598.

Haines, R. W. (1952). The shoulder joint of lizards and the primitive reptilian shoulder mechanism. *Journal of Anatomy*, *86*, 412–422.

Heers, A. M., & Dial, K. P. (2012). From extant to extinct: Locomotor ontogeny and the evolution of avian flight. *Trends in Ecology & Evolution*, *27*, 296–305.

Hirschmann, M. T., & Müller, W. (2015). Complex function of the knee joint: The current understanding of the knee. *Knee Surgery, Sports Traumatology, Arthroscopy*, *23*, 2780–2788.

Holmes, R. (1977). The osteology and musculature of the pectoral limb of small captorhinids. *Journal of Morphology*, *152*, 101–140.

Hopson, J. A. (2015). Fossils, trackways, and transitions in locomotion: A case study of *Dimetrodon*. In K. P. Dial, N. H. Shubin, & E. L. Brainerd (Eds.), *Great transformations in vertebrate evolution*. University of Chicago Press.

Hutson, J. D., & Hutson, K. N. (2015). An examination of forearm bone mobility in *Alligator mississippiensis* (Daudin, 1802) and *Struthio camelus* Linnaeus, 1758 reveals that *archaeopteryx* and dromaeosaurs shared an adaptation for gliding and/or flapping. *Geodiversitas*, *37*, 325–344.

Jenkins, F. A., Jr. (1971). The postcranial skeleton of African cynodonts. *Bulletin of the Peabody Museum of Natural History*, *36*, 1–216.

Jenkins, F. A., Jr. (1973). The functional anatomy and evolution of the mammalian Humero-ulnar articulation. *American Journal of Anatomy*, *137*, 281–298.

Jenkins, F. A., Jr. (1993). The evolution of the avian shoulder joint. *American Journal of Science*, *293-A*, 253–267.
Jenkins, F. A., Jr., & Goslow, G. E., Jr. (1983). The functional anatomy of the shoulder of the Savannah monitor lizard (*Varanus exanthematicus*). *Journal of Morphology*, *175*, 195–216.
Jones, K. E., Brocklehurst, R. J., & Pierce, S. E. (2021). AutoBend: An automated approach for estimating intervertebral joint function from bone-only digital models. *Integrative Organismal Biology*, *3*, obab026.
Jones, K. E., Dickson, B. V., Angielczyk, K. D., & Pierce, S. E. (2021). Adaptive landscapes challenge "lateral-to-sagittal" paradigm for mammalian vertebral evolution. *Current Biology*, *31*, 1–10.
Kambic, R. E., Biewener, A. A., & Pierce, S. E. (2017). Experimental determination of three-dimensional cervical joint mobility in the avian neck. *Frontiers in Zoology*, *14*, 37.
Kambic, R. E., Roberts, T. J., & Gatesy, S. M. (2017). 3-D range of motion envelopes reveal interacting degrees of freedom in avian hind limb joints. *Journal of Anatomy*, *231*, 906–920.
Kemp, T. S. (1978). Stance and gait in the hindlimb of a therocephalian mammal-like reptile. *Journal of Zoology*, *186*, 143–161.
Lai, P. H., Biewener, A. A., & Pierce, S. E. (2018). Three-dimensional mobility and muscle attachments in the pectoral limb of the Triassic cynodont *Massetognathus pascuali* (Romer, 1967). *Journal of Anatomy*, *232*, 383–406.
Landsmeer, J. M. F. (1983). The mechanism of forearm rotation in *Varanus exanthematicus*. *Journal of Morphology*, *175*, 119–130.
Maidment, S. C. R., Bates, K. T., Falkingham, P. L., VanBuren, C., Arbour, V., & Barrett, P. M. (2014). Locomotion in ornithischian dinosaurs: An assessment using three-dimensional computational modelling. *Biological Reviews*, *89*, 588–617.
Mallison, H. (2010). CAD assessment of the posture and range of motion of *Kentrosaurus aethiopicus* Hennig 1915. *Swiss Journal of Geosciences*, *103*, 211–233.
Manafzadeh, A. R. (2020). A practical guide to measuring *ex vivo* joint mobility using XROMM. *Integrative Organismal Biology*, *2*, obaa041.
Manafzadeh, A. R., & Gatesy, S. M. (2020). A coordinate-system-independent method for comparing joint rotational mobilities. *Journal of Experimental Biology*, *223*, jeb227108.
Manafzadeh, A. R., & Gatesy, S. M. (2021). Paleobiological reconstructions of articular function require all six degrees of freedom. *Journal of Anatomy*, *239*, 1516–1524.
Manafzadeh, A. R., & Gatesy, S. M. (2022). Advances and challenges in paleobiological reconstructions of joint mobility. *Integrative and Comparative Biology*, *2022*, icac008.
Manafzadeh, A. R., & Padian, K. (2018). ROM mapping of ligamentous constraints on avian hip mobility: Implications for extinct ornithodirans. *Proceedings of the Royal Society of London, Series B*, *285*, 20180727.
Miner, R. W. (1925). The pectoral limb of *Eryops* and other primitive tetrapods. *Bulletin of the American Museum of Natural History*, *51*, 145–312.
Möller, T., & Trumbore, B. (1997). Fast, minimum storage ray-triangle intersection. *Journal of Graphics Tools*, *2*, 21–28.
Molnar, J. L., Hutchinson, J. R., Diogo, R., Clack, J. A., & Pierce, S. E. (2021). Evolution of forelimb musculoskeletal function across the fish-to-tetrapod transition. *Science Advances*, *7*, eabd7457.
Nyakatura, J. A., Melo, K., Karakasiliotis, K., Allen, V. R., Andikfar, A., Andrada, E., Arnold, P., Lauströer, J., Hutchinson, J. R., Fischer, M. S., & Ijspeert, A. J. (2019). Reverse-engineering the locomotion of a stem amniote. *Nature*, *565*, 351–355.
Ostrom, J. H. (1969). Osteology of *Deinonychus antirrhopus*, an unusual theropod from the lower cretaceous of Montana. *Bulletin of the Peabody Museum of Natural History*, *30*, 1–165.
Parrish, J. M. (1986). Locomotor adaptations in the hindlimb and pelvis of the Thecodontia. *Hunteria*, *1*, 1–35.
Pataky, T. C., & Challis, J. H. (2020). Using directional statistics to test hypotheses regarding rigid body attitude: Comparison to univariate and multivariate cardan angle tests. *Journal of Biomechanics*, *111*, 109976.
Paul, G. S. (1998). Limb design, function and running performance in ostrich-mimics and tyrannosaurs. *Gaia*, *15*, 257–270.
Peters, S. E., & Goslow, G. E., Jr. (1983). From salamanders to mammals: Continuity in musculoskeletal function during locomotion. *Brain, Behavior and Evolution*, *22*, 191–197.
Pierce, S. E., Clack, J. A., & Hutchinson, J. R. (2012). Three-dimensional limb joint mobility in the early tetrapod *Ichthyostega*. *Nature*, *486*, 523–526.
Pierce, S. E., Lamas, L. P., Pelligand, L., Schilling, N., & Hutchinson, J. R. (2020). Patterns of limb and epaxial muscle activity during walking in the fire salamander, *Salamandra salamandra*. *Integrative Organismal Biology*, *2*, obaa015.
Regnault, S., Fahn-Lai, P., & Pierce, S. E. (2021). Validation of an echidna forelimb musculoskeletal model using XROMM and diceCT. *Frontiers in Bioengineering and Biotechnology*, *9*, 751518.
Regnault, S., & Pierce, S. E. (2018). Pectoral girdle and forelimb musculoskeletal function in the echidna (*Tachyglossus aculeatus*): Insights into mammalian locomotor evolution. *Royal Society Open Science*, *5*, 181400.
Richards, H. L., Bishop, P. J., Hocking, D. P., Adams, J. W., & Evans, A. R. (2021). Low elbow mobility indicates unique forelimb posture and function in a giant extinct marsupial. *Journal of Anatomy*, *238*, 1425–1441.
Romer, A. S. (1922). The locomotor apparatus of certain primitive and mammal-like reptiles. *Bulletin of the American Museum of Natural History*, *46*, 517–606.
Romer, A. S., & Price, L. I. (1940). Review of the Pelycosauria. *Special Papers of the Geological Society of America*, *28*, 1–538.
Senter, P., & Robins, J. H. (2005). Range of motion in the forelimb of the theropod dinosaur *Acrocanthosaurus atokensis*, and implications for predatory behaviour. *Zoological Journal of the Linnean Society*, *266*, 307–318.
Stevens, K. A., & Parrish, J. H. A. (1999). Neck posture and feeding habits of two Jurassic sauropod dinosaurs. *Science*, *284*, 798–800.
Turner, M. L., & Gatesy, S. M. (2021). Alligators employ intermetatarsal reconfiguration to modulate plantigrade ground contact. *Journal of Experimental Biology*, *224*, jeb242240.
Walker, W. F. (1973). The locomotor apparatus of testudines. In C. Gans & T. S. Parsons (Eds.), *Biology of the Reptilia*. Academic Press.
Watson, D. M. S. (1917). The evolution of the tetrapod shoulder girdle and fore-limb. *Journal of Anatomy*, *52*, 1–63.
Yamaguchi, G. T., & Zajac, F. E. (1989). A planar model of the knee joint to characterize the knee extensor mechanism. *Journal of Biomechanics*, *22*, 1–10.

SUPPORTING INFORMATION

Additional supporting information can be found online in the Supporting Information section at the end of this article.

How to cite this article: Bishop, P. J., Brocklehurst, R. J., & Pierce, S. E. (2023). Intelligent sampling of high-dimensional joint mobility space for analysis of articular function. *Methods in Ecology and Evolution*, *14*, 569–582. https://doi.org/10.1111/2041-210X.14016